Volume 10 · No. 2 – January 29 2014

NANO MICRO

small

www.small-journal.com

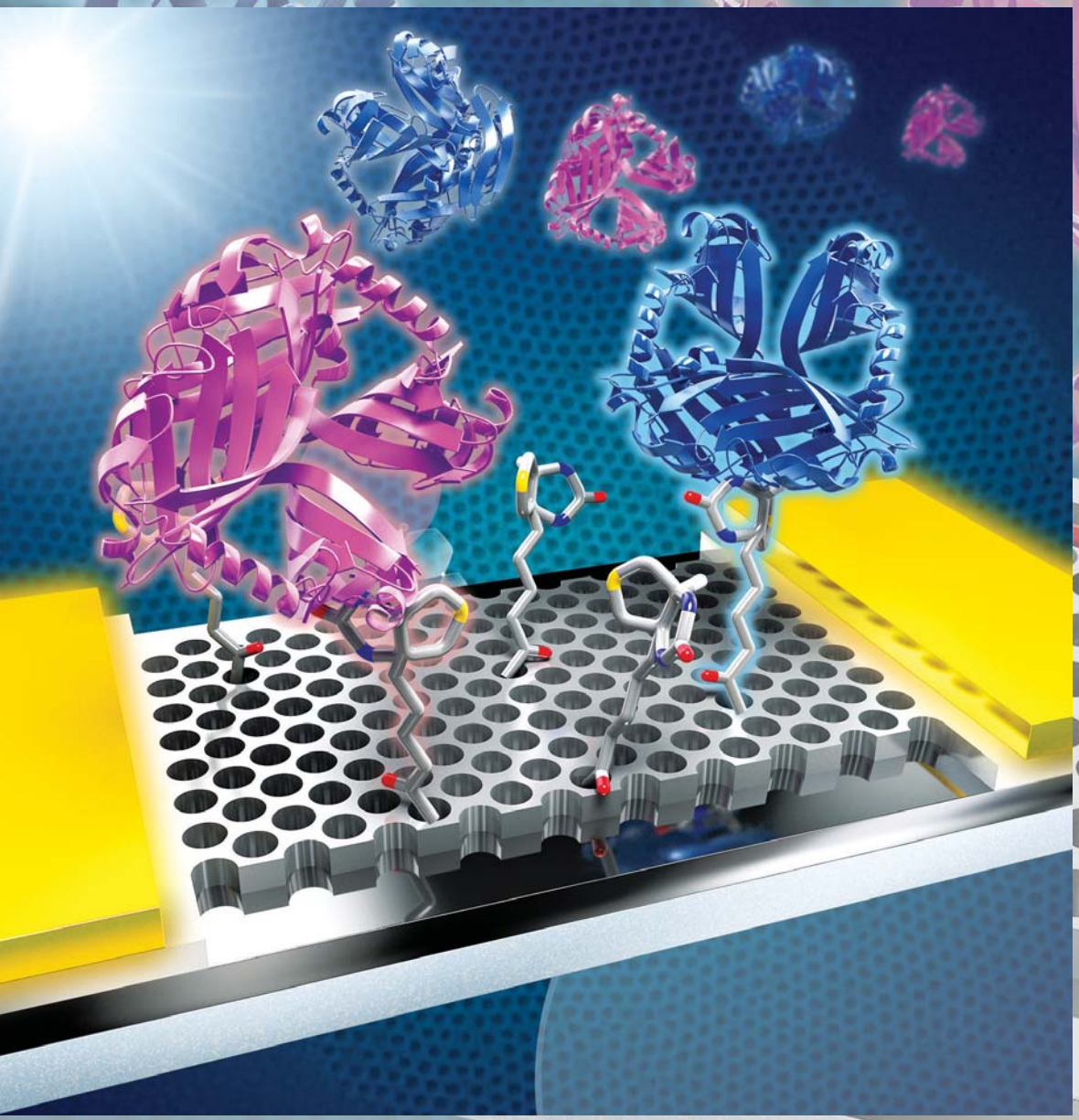

2/2014

WILEY-VCH

Electrical Biomolecule Detection Using Nanopatterned Silicon via Block Copolymer Lithography

S. O. Kim, K. J. Lee, and co-workers

small
NANO MICRO

Electrical Biomolecule Detection Using Nanopatterned Silicon via Block Copolymer Lithography

Chang Kyu Jeong, Hyeong Min Jin, Jae-Hyuk Ahn, Tae Jung Park, Hyeon Gyun Yoo, Min Koo, Yang-Kyu Choi, Sang Ouk Kim, and Keon Jae Lee**

An electrical biosensor exploiting a nanostructured semiconductor is a promising technology for the highly sensitive, label-free detection of biomolecules via a straightforward electronic signal. The facile and scalable production of a nanopatterned electrical silicon biosensor by block copolymer (BCP) nanolithography is reported. A cost-effective and large-area nanofabrication, based on BCP self-assembly and single-step dry etching, is developed for the hexagonal nanohole patterning of thin silicon films. The resultant nanopatterned electrical channel modified with biotin molecules successfully detects the two proteins, streptavidin and avidin, down to nanoscale molarities (≈1 nM). The nanoscale pattern comparable to the Debye screening length and the large surface area of the three-dimensional silicon nanochannel enable excellent sensitivity and stability. A device simulation confirms that the nanopatterned structure used in this work is effective for biomolecule detection. This approach relying on the scalable self-assembly principle offers a high-throughput manufacturing process for clinical lab-on-a-chip diagnoses and relevant biomolecular studies.

1. Introduction

The detection of biological elements, such as biomarkers,[1] viruses,[2] and pathogens,[3] is crucial for the early diagnosis and treatment of human diseases. Although enzyme-linked immunosorbent assay (ELISA) has been extensively used for biosensing, it is well known that ELISA has critical limitations, such as complicated labeling steps, high analyte concentration requirements,[4] and incompatibility with electronic detection caused by difficulties of signal conversion. Various types of biosensors, including thermometric,[5] magnetic,[6] piezoelectric,[7] optical,[8,9] and electrical[10–14] biosensors, have been developed to surpass such limitations. Among them, the electrical biosensor using semiconductor

C. K. Jeong, H. G. Yoo, Dr. M. Koo, Prof. K. J. Lee
Department of Materials Science and Engineering
Korea Advanced Institute of Science and Technology (KAIST)
291 Daehak-ro, Yuseong-gu, Daejeon 305–701, Republic of Korea
E-mail: keonlee@kaist.ac.kr
H. M. Jin, Prof. S. O. Kim
Center for Nanomaterials and Chemical Reactions
Institute for Basic Science (IBS)
Department of Materials Science and Engineering
Korea Advanced Institute of Science and Technology (KAIST)
291 Daehak-ro, Yuseong-gu, Daejeon 305–701, Republic of Korea
E-mail: sangouk.kim@kaist.ac.kr

DOI: 10.1002/smll.201301202

J.-H. Ahn, Prof. Y.-K. Choi
Department of Electrical Engineering
Korea Advanced Institute of Science
and Technology (KAIST)
291 Daehak-ro, Yuseong-gu, Daejeon 305–701,
Republic of Korea
Dr. T. J. Park[+]
BioProcess Engineering Research Center
Center for Systems and Synthetic Biotechnology
Institute for the BioCentury
Korea Advanced Institute of Science and Technology (KAIST)
291 Daehak-ro, Yuseong-gu, Daejeon 305–701, Republic of Korea
[+]Present address: Department of Chemistry, Chung-Ang University, 84 Heukseok-ro, Dongjak-gu, Seoul 156-756, Republic of Korea

nanomaterials has been regarded as a strong candidate for next-generation biosensors due to its high sensitivity, rapid diagnosis without labeling steps, and compatibility with integrated circuits.[15–17]

The nanostructured channel in a field-effect transistor (FET) has been considered for potential use in high-performance electrical biosensors. The high sensitivity is facilitated by the nano-dimensional channel, which is comparable to the Debye screening length[18] and size of biomolecules.[15,19] To date, many research groups have reported bottom-up methods for fabrication of carbon materials (e.g., carbon nanotubes and graphene)[20,21] or silicon nanowires[2,12,22] for the high sensitivity of biosensors. However, these bottom-up approaches revealed drawbacks including the inaccurate positioning of nanomaterials, the poor uniformity of doping levels, and the low integration density for ultimate commercialization.[13] In contrast, top-down approaches, such as electron-beam lithography, have been successfully employed for ultrafine nanoscale biosensors, including those reported in our previous studies.[11,14] Nonetheless, the major limitation of top-down electron-beam nanofabrication lies in the high cost and extremely low throughput, which are inherently incompatible with large-scale manufacturing.[15]

Block copolymer (BCP) self-assembly, which is generally driven by the microphase separation of covalently linked incompatible polymer blocks, is able to form dense and ordered pattern arrays of even sub-10 nm features.[23,24] BCP self-assembly is considered to be a powerful and viable tool for nanolithography due to its excellent scalability, high pattern precision, and compatibility with the conventional complementary metal oxide semiconductor process.[25,26] Many research groups have exploited BCP self-assembly for a variety of materials and applications.[27–31] For example, we have introduced BCP lithography for the nanoscale patterning of arbitrary substrate materials[32,33] up to wafer scale with a few tens of nanometers-scale feature sizes.

Herein, we report the electrical detection of biomolecules using an ultrathin Si nanomesh patterned by BCP lithography. Polystyrene-*block*-poly(methyl methacrylate) (PS-*b*-PMMA) thin films with vertically hexagonal cylinder morphology are employed as templates for single-step SF_6 dry etching to generate a large-area Si nanomesh structure of sub-20 nm-scale features. The nanomesh channel enables the biosensor to monitor pH changes and detects two proteins of similar structures: streptavidin and avidin. The performance of the nanopatterned biosensor is compared with that of the non-patterned counterpart to demonstrate the advantage of the nanopatterned structure for detection sensitivity. Technology computer-aided design (TCAD) device simulation is performed to theoretically support the merits of the nanostructured semiconductor over non-patterned devices for biomolecule detection.

2. Results and Discussion

The overall fabrication scheme for the nanopatterned electrical biosensor is illustrated in **Figure 1**. The high-level boron doping of the source and drain (S/D) regions is

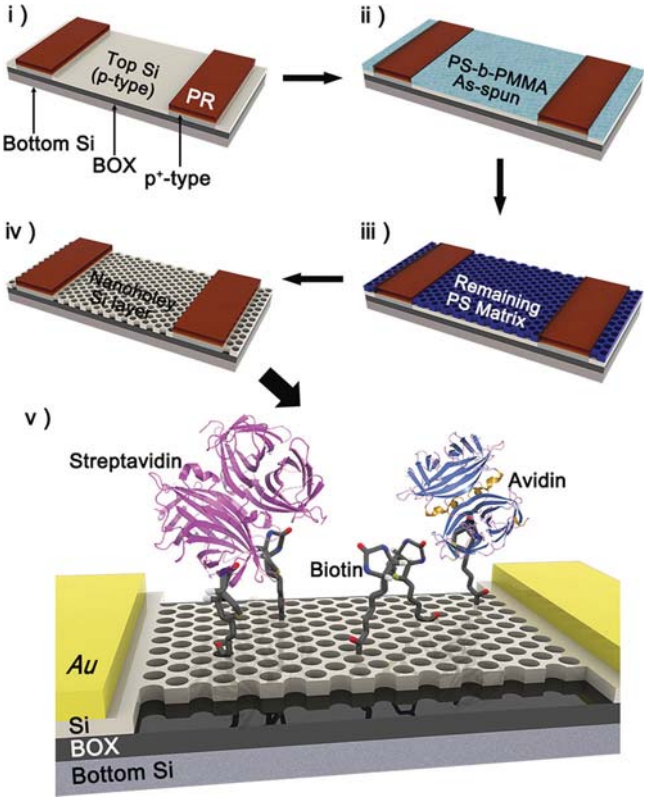

Figure 1. Schematic process for a nanopatterned electrical biosensor, including i) boron doping, ii) BCP spin-casting and self-assembly, iii) PMMA domain removal, and iv) pattern transfer to the top Si layer. v) An FET-based biosensor is functionalized with biotin molecules for detecting streptavidin or avidin protein (BOX = buried oxide).

performed on an ultrathin Si layer (≈25 nm) of a silicon-on-insulator (SOI) wafer by ion implantation. After covering S/D regions with a photoresist (PR; Figure 1-i), the top Si surface is covalently modified with poly(styrene-*random*-methyl methacrylate) (P(S-*r*-MMA)) copolymer. A PS-*b*-PMMA thin film is spin-cast and thermally annealed (250 °C) to induce microphase separation (Figure 1-ii). The BCP thin film spontaneously assembles into the morphology of vertically hexagonal cylinders on the neutrally modified surface due to an identical interfacial tension to PS and PMMA. The PMMA cylindrical nanodomains are selectively removed by the sequential treatments of acetic acid solution and O_2 plasma (Figure 1-iii). The remaining PS template after PMMA etching is employed as a nanopatterned mask for the following dry etching of the underlying Si layer. A single-step inductively coupled plasma reactive ion etching (ICP-RIE) using SF_6 gas is applied to the pattern transfer of PS template morphology into the top Si layer (Figure 1-iv). Notably, such a well-defined hexagonal nanohole PS template endures the harsh dry etching during the complete etching of the Si layer,[34] which is differentiated from previous BCP studies that employed complicated multistep processes, including metal mask deposition. After the complete removal of the remaining PS nanotemplate and PR patterns, the formation of the channel region and metal contacts is carried out by using conventional photolithography and wet

small NANO MICRO

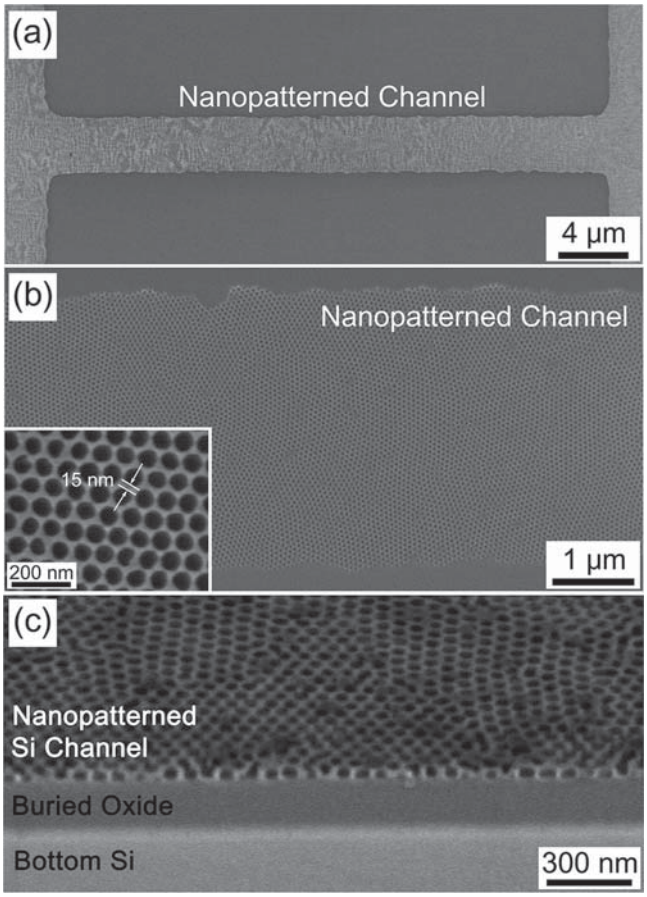

Figure 2. a) SEM image of a nanopatterned Si channel. Moiré fringes over the entire channel region demonstrate the uniformity of the nanopatterned Si structure. b) Magnified SEM image of the nanopatterned Si channel. c) Cross-sectional SEM image of the hexagonal nanohole morphology of the top Si layer (≈25 nm thickness).

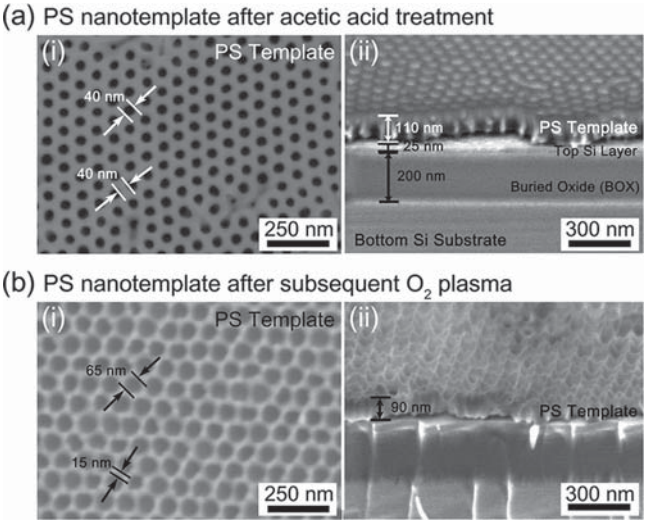

Figure 3. The nanomesh PS template before Si etching for pattern transfer. a) Plane view (i) and 60° tilted view (ii) of SEM image of remaining PS template after acetic acid wet treatment for PMMA elimination (average diameter of nanoholes: 40 nm, average width between neighboring holes: 40 nm, thickness of PS template: 110 nm). b) Plane view (i) and 60° tilted view (ii) of SEM image of remaining PS template after subsequent O_2 plasma treatment for removing residual PMMA and widening the PS nanotemplate holes (average diameter of nanoholes: 65 nm, average width between neighboring holes: 15 nm, thickness of PS template: 90 nm).

etching. For the last stage, the nanochannel area is sequentially functionalized with a (3-aminopropyl)triethoxysilane (APTES) self-assembled monolayer (SAM) and biotin 3-sulfo-*N*-hydroxysuccinimide ester (sulfo-NHS-biotin) for specific binding with the streptavidin or avidin.[35] Figure 1-v schematically presents the biosensor with a nanopatterned Si channel functionalized by biotin molecules. The biotin–streptavidin/avidin system used in our experiments has served extensively as a standard model for protein–ligand interactions.[21]

The nanopatterned Si channel fabricated by BCP lithography is observed with scanning electron microscopy (SEM). Moiré fringes caused by the interference between instrumental aliasing and sample grating are shown in **Figure 2**a,[36] which confirms the uniformity of nanopattern transfer over the entire channel region. In this work, a BCP template with a PS mesh-hole diameter of ≈40 nm is employed (**Figure 3**a-i and 3a-ii).[37,38] The average hole diameter of PS patterns increases up to ≈65 nm by O_2 over-etching (Figure 3b-i and 3b-ii), which realizes a Si nanomesh of ≈15 nm after the pattern transfer (Figure 2b). This additional etching of PS template for the narrow Si nanopattern is important to fabricate the nanoscale biosensor. Figure 2c is a cross-sectional SEM image of a nanopatterned channel, which indicates that the dry etching successfully transfers the nanopattern of PS mesh onto the entire top Si layer.[25,39] The nanomesh design of the Si channel is comparable to the screening length of analyte charges and thus ensures high sensing resolution for biomolecule detection.

Figure 4a depicts the chemical modification steps of the nanopatterned Si channel for biosensing. The surface terminal group of an APTES-treated Si channel is composed of primary amines ($-NH_2$), protonated amines ($-NH_3^+$), and hydroxyl groups (–OH), as confirmed by X-ray photoelectron spectroscopy (XPS) (Figure 4b). For streptavidin or avidin detection, sulfo-NHS-biotin is linked with the amine group of APTES on the Si channel. There are four biotin-binding pockets in the proteins, but one or two of them can be bound to the immobilized biotin.[35] The variation of the current recording through the nanopatterned channel upon surface functionalization is plotted in Figure 4c. The current decreases upon silanization due to the positive charge of $-NH_3^+$ groups of APTES. During the biotinylation step, the sulfo-NHS-biotin is immobilized through reaction with the protonated amine as well as the primary amine of APTES-SAM.[35] As a result, the density of protonated amine groups is considerably reduced on the nanopatterned Si, which consequently increases the current flow.

The influence of the nanopattern on charge detection sensitivity was evaluated by the conductance change of the APTES-modified Si nanochannel with pH (**Figure 5**a). The $-NH_3^+$ groups induced by the protonation of $-NH_2$ at low pH[12] are able to deplete holes in a p-type nanopatterned Si channel and thereby reduce the conductance. By contrast,

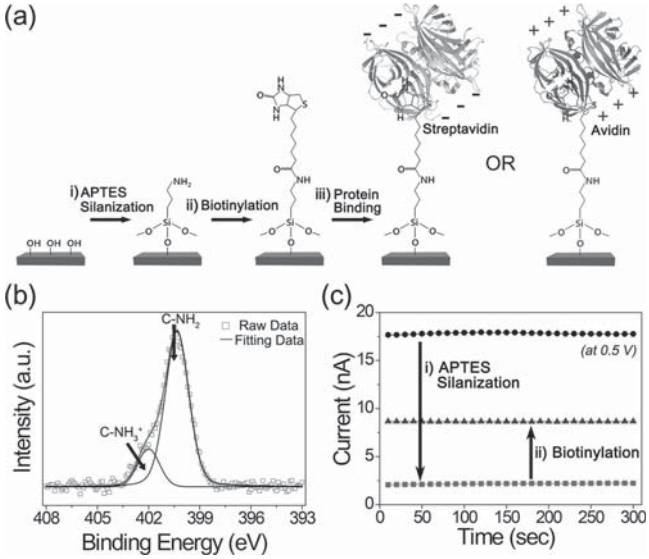

Figure 4. a) Schematic diagram of the chemical functionalization method for streptavidin or avidin protein binding onto the biotinylated Si channel. i) Formation of APTES-SAM through silanization. ii) Biotinylation using sulfo-NHS-biotin linked with immobilized APTES-SAM. iii) Biotin-binding protein, streptavidin (negatively charged) or avidin (positively charged), attaches to the biotinylated Si channel. b) N1s XPS spectra of APTES immobilized on the Si channel: C–NH_2 peak (399.9 eV) and C–NH_3^+ peak (401.9 eV). c) The current changes of the nanopatterned biosensor are plotted during sequential surface functionalization steps. The current decreases after APTES silanization due to the formation of –NH_3^+ charges. On the contrary, the fraction of –NH_3^+ chemical groups is considerably reduced by the subsequent biotinylation step, which induces the increase of current flow.

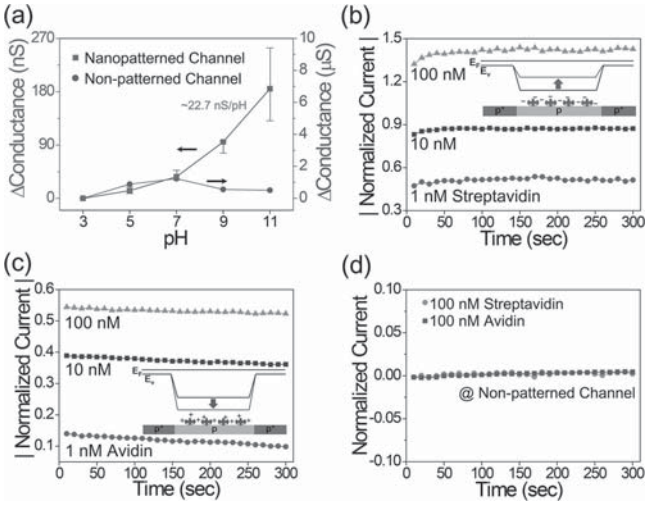

Figure 5. a) Conductance changes of nanopatterned (square symbols) and non-patterned channels (circle symbols) versus pH. The range-bars of conductance changes in the nanopatterned channel demonstrate the reliability of nanochannel-based charge detection. b) Normalized current changes upon streptavidin binding at the nanopatterned channel. The inset illustrates the variation of valence band state of the channel upon streptavidin binding. c) Normalized current changes upon avidin binding at the nanopatterned channel. The inset illustrates the variation of valence band state after avidin binding. d) Normalized current changes of the nonpatterned channel upon protein binding. No noticeable current change was observed. The normalized currents are calculated from $(I–I_0)/I_0$ and treated as absolute values (I_0: initial current level before protein binding; I: changed current after protein binding).

at a high pH, –NH_3^+ and –OH groups are deprotonated to –NH_2 and –O^-, respectively (Figure S2, Supporting Information). The deprotonation negatively modifies the Si surface, which causes the increase of conductance (Figure 5a).[12] Meanwhile, there is no noticeable current change with pH on the non-patterned device, as the short screening length of surface functional groups hardly influences the entire bulk channel. A pH sensitivity of about 22.7 nS per pH unit is obtained in the nanopatterned channel, which is comparable to previous reports.[2] The small-scale range-bars of conductance change in the nanopatterned channel indicate the good reproducibility and reliability of our nanochannel-based charge detection.

Figure 5b and 5c depict the detection of streptavidin and avidin, which have almost identical protein structures and similar affinity for biotin.[10] However, their opposite charges at neutral pH caused by their different isoelectric points (pI)—streptavidin pI ≈5.6 and avidin pI ≈10.5—enable their distinguishable detection.[40] Figure 5b shows that the current level of the nanomesh biosensor increases while streptavidin proteins with negative charges are bound to the biotinylated channel in a phosphate-buffered saline (PBS, pH 7.4) solution for 5 min. This current increment is attributed to the hole accumulation by negative charges and the potential barrier lowering in the nanomesh p-type channel, as illustrated by the inset of Figure 5b. By contrast, the current level of the nanopatterned biosensor decreases when avidin proteins are bound to the channel. The positively charged proteins induce the hole depletion and the potential barrier rise, as indicated in the inset of Figure 5c. Streptavidin and avidin concentrations down to 1 nM are detectable by our nanopatterned biosensor. Although this detection sensitivity is considerably high, a few previous works have demonstrated ultrahigh sensitivity down to pico- and femtoscale molarity.[10,16] We believe that our nanopatterned biosensor could improve the detection sensitivity by adopting the advanced electrical biosensing utilized in the previous works, such as the gate-modulated ion-sensitive FET (ISFET) for the electrical inversion layer,[41] microfluidic system for real-time detection,[42] and/or anisotropic Si etching for the highly binding site of surface crystalline orientation.[16] Unlike the nanopatterned biosensor, a non-patterned device rarely shows the current change, because the hole accumulation or depletion by protein binding is negligible compared to the total carrier flow of the bulk channel (Figure 5d). These results clearly confirm that the nanopatterned structure is more suitable for the highly sensitive biosensor than the non-patterned counterpart.

Several control tests were carried out to confirm that the strepatavidin/avidin detection is attributable to the specific binding on the biotinylated surface. The nanopatterned device without surface functionalization exhibits no current change after incubation in proteins, as shown in **Figure 6**a. Also, there are negligible changes in the current flow when human serum albumin (HSA) is added as a nonspecific protein for biotin (Figure 6b). The addition of streptavidin

NANO MICRO small

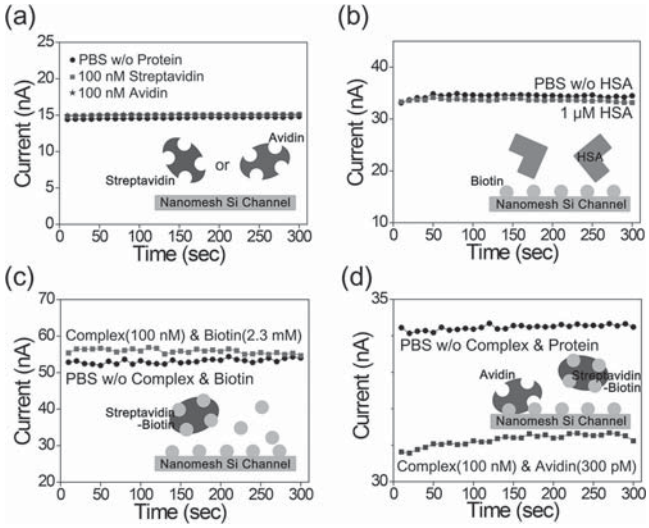

Figure 6. a) Current levels of the nanomesh channel without biotinylation. b) Current characteristics of the biotinylated nanomesh device with the nonspecific protein, HSA. c) Current levels of the nanopatterned and biotinylated channel in the presence of excess biotin molecules and preblocked streptavidin–biotin complex. d) Current change of the biotinylated nanomesh Si channel upon mixing the solution with 300 pM avidin and preblocked streptavidin–biotin complex.

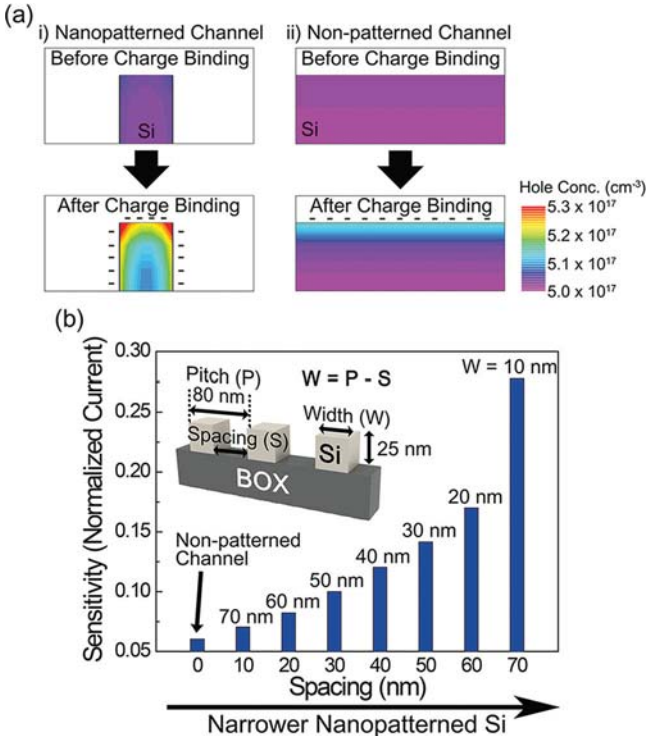

Figure 7. Three-dimensional TCAD simulation of a nanostructured Si biosensor. a) Cross-sectional views of simulated hole concentration at the i) nanopatterned and ii) nonpatterned channels. A dramatic change of carrier concentration occurs in the nanomesh structure, whereas there is relatively less concentration change in the nonpatterned one after negative charge binding. b) Sensitivity of biosensor versus nanochannel width. The sensitivity is evaluated by the normalized current, $(I-I_0)/I_0$. The inset is a cross-sectional illustration of the nanomesh channel employed in the simulation.

preblocked by an extremely excessive biotin concentration (≈2.3 mM) leads to slight deviation in the current–time plot, as illustrated in Figure 6c. This insignificant fluctuation results from unexpected interactions of excess biotin molecules with APTES-SAM due to the small size of biotin compared to the protein. By contrast, the mixed solution with unblocked avidin and biotin-blocked streptavidin reduces the current of the nanomesh biosensor (Figure 6d). This result indicates that our nanopatterned biosensor could detect avidin even down to 300 pM, while a reliable detection limit is suggested to be around 1 nM. Consistently, streptavidin can also be detected down to about 300 pM (Figure S3a). Below ≈100 pM, however, the device did not detect either streptavidin or avidin (Figures S3a and S3b). We note that that the current change for streptavidin sensing is slightly larger than that for avidin in the above measurements. This discrepancy is caused by the modification of binding affinity to biotin. The affinities of avidin and streptavidin for biotin are originally similar. However, avidin may have a reduced affinity if biotin is conjugated to another moiety or molecule. On the contrary, streptavidin shows a similar affinity to the conjugated biotin.[43] The biotin immobilized on the device channel can be regarded as a conjugated one and may significantly decrease avidin binding. In addition, avidin frequently suffers from aggregation via nonspecific binding, which is attributed to the high pI as well as the presence of acetylglucosamine and mannose in the protein structure.[44] These effects may cause a smaller current change for avidin detection, as previously reported by others.[40]

The sensitivity of the nanopatterned biosensor is investigated theoretically with a TCAD device simulation.[11,45] **Figure 7**a shows the charge effect of biomolecules depending on Si structure.[19] The dramatic change of hole concentration in Figure 7a-i is induced in the three-dimensional surfaces of the nanopatterned Si channel after the negative charge binding corresponding to streptavidin. On the contrary, weak carrier variation occurs only at the top surface of the nonpatterned biosensor (Figure 7a-ii). These results are caused by the three-dimensional charge effect[46] and the nanoscale channel width, the length scale of which is comparable to the Debye screening length of a biomolecule.[11] Figure 7b shows the sensitivity (normalized current) versus spacing size between two Si pillars (cross section of nanopatterned Si); the pitch and height of Si pillars are fixed at 80 and 25 nm, respectively. A large-spacing (narrow Si nanopillar) biosensor has a high sensitivity when negative surface charges are attached. It confirms that our nanomesh device is more effective for biomolecule detection than a non-patterned one. We note that the significant enhancement of sensitivity at sub-20 nm width (W) results from the volume accumulation.[47] These results support the advantage of the nanopatterned structure for biomolecule detection. The case of positive charge binding corresponding to avidin is demonstrated in Figure S4.

3. Conclusion

We have demonstrated a highly sensitive electrical biosensor with a sub-20 nm-scale nanomesh semiconductor structure

fabricated using BCP lithography. Precise, simple, and cost-effective nanofabrication can be realized through the facile BCP nanopatterning and one-step dry etching. The nanomesh electrical biosensor is able to selectively detect oppositely charged proteins, such as streptavidin and avidin, down to nanoscale molarities. We confirmed the nanopatterning effects on the sensitivity of the electrical biosensor by TCAD device simulation. The simulated results are consistent with the experimental measurements, which are anticipated from the three-dimensional charge effect and a nanostructure comparable to the Debye screening length of biomolecules. This work suggests that BCP lithography is potentially useful for various biomedical applications, such as disease diagnoses, biological kinetic studies, and even lab-on-a-chip technologies.

4. Experimental Section

Device Fabrication: Silicon-on-insulator (SOI) wafers (p-type doped; SOITEC) were used with top Si thickness of 110 nm and a buried oxide (BOX) thickness of 200 nm. The original top Si was thinned down to 25 ± 3 nm by dry oxidation and wet etching. The thinned Si layer was doped with boron by ion implantation (dose 10^{15} cm^{-2}, which means $\approx 10^{18}$ cm^{-3}, low energy 3 eV), followed by annealing at 1050 °C. A 500 nm SiO_2 implant mask was prepared by plasma-enhanced chemical vapor deposition (PECVD), photolithography, and ICP dry etching (ICP-RIE, 10 mTorr, O_2/C_4F_8). Source and drain (S/D) regions (p^+-type) were formed by additional boron ion implantation (dose 10^{18} cm^{-2}, 3 eV). PR patterns were then defined to protect the S/D regions from the subsequent BCP nanopattern transfer (Figure S1-i). After the removal of the SiO_2 implant mask by HF, BCP lithography was employed for nanopatterning of the top Si layer (see the next Experimental Section). After the pattern transfer to the top Si, the PR patterns covering S/D regions were removed by piranha solution (H_2SO_4/H_2O_2 = 3:1). The isolation of the S/D regions and channel was conducted by photolithography and ICP-RIE (10 mTorr, O_2/SF_6). The nanopatterned Si channels were 2–4 μm in width and 25 μm in length. S/D metal contacts were defined by a standard lift-off process using Cr/Au (10/200 nm) metal layers deposited by radio-frequency sputtering (Figure S1-vi). Lastly, the device was passivated by spin-cast SU-8 layers (Micro Chem.), except for the channel and metal contact pads. The electrical measurements were performed by Keithley 4200-SCS (DC voltage sweep) and Keithley 4225-RPM (pulse generator, waveform capture of voltage) instruments. The conductance and current levels of the biosensor were measured at a source voltage of 1.5–2.5 V. The three-dimensional device simulation results were extracted from the commercialized semiconductor simulator ATLAS (SILVACO). Boron doping concentrations of the channel and S/D regions were defined as 5×10^{17} and 1×10^{20} cm^{-3}, respectively. The thickness of the top Si layer was 25 nm with 2 nm native SiO_2 layer on the entire three-dimensional structure. The pitch between hole centers was fixed at 80 nm and the spacing between neighboring holes was varied from 0 to 70 nm. The surface charge density was fixed as 1×10^{10} cm^{-2}. Some deviations with experiments could be caused by the carrier collisions at nanoholes, the number of patterns, and the SAM surface effects, which could not be considered in the simulation.

BCP Nanopatterning and Pattern Transfer Etching: The SOI wafer is cleaned by ultraviolet-ozone (UVO) treatment for 30 minutes. The cleaned surface was then neutrally modified by covalent functionalization with a hydroxyl-terminated P(S-*r*-MMA) copolymer brush layer. The P(S-*r*-MMA) solution (1% w/w in toluene) was spin-cast onto the surface and reacted at 160 °C overnight in a vacuum. PS-*b*-PMMA (average molecular weight M_n = 200 kg mol^{-1}, 140–60 kg mol^{-1} for PS and PMMA blocks, respectively; Polymer Source) and BCP powder were dissolved in toluene (3% w/w). A PS-*b*-PMMA thin film was formed by spin-casting at 3000 rpm (Figure S1-ii). Hexagonally ordered PMMA cylinder domain arrays were induced by annealing at 250 °C overnight in a vacuum (Figure S1-iii). After UV radiation (4 J) for the simultaneous cross-linking of PS and the degradation of PMMA, PMMA cylindrical nanodomains were selectively removed by acetic acid (Junsei) for 10 min. The PMMA residues were entirely swept out by brief O_2 plasma (800 mTorr, 50 W) (Figure S1-iv). The O_2 plasma treatment also considerably widened the nanohole size of the PS template. The remaining nanomesh PS film acted as a mask for the following etching of the top Si layer by ICP-RIE (10 mTorr, 25 sccm SF_6). After the pattern transfer, the residual PS film was eliminated by O_2 plasma treatment (10 mTorr, 60 W) and piranha solution (Figure S1-v).

Surface Functionalization for Biomolecule Detection: The nanopatterned Si channel was hydroxylated by UVO treatment for 30 min. The sample was then submerged in a 2% v/v APTES (Sigma–Aldrich) solution of anhydrous ethanol (Sigma–Aldrich) for 12 h at ambient temperature (Figure 4a-i). The silanized surface was rinsed with diluted acetic acid and ethanol. After baking the specimen at 120 °C for 10 min, sulfo-NHS-biotin (Sigma–Aldrich) dissolved in deionized water (1 mg mL^{-1}) was dropped on the channel region, followed by incubation at 37 °C for 2 h (Figure 4a-ii). The device was immersed in 1% v/v blocker bovine serum albumin (BSA; Pierce Biotechnology) in PBS (10 mM phosphate, 138 mM NaCl, 2.7 mM KCl, pH 7.4; Sigma–Aldrich) for 1 h to fill the cavities of the biotin-linked surface. Streptavidin and avidin (Sigma–Aldrich) were dissolved in the 0.01× PBS solution. The protein solutions were dropped and incubated on the biotinylated channel surface at room temperature for 15 min (Figure 4a-iii). The HSA (Sigma–Aldrich) for the control test was treated by a similar protocol to that of streptavidin and avidin.

Supporting Information

Supporting Information is available from the Wiley Online Library or from the author.

Acknowledgements

C.K.J. and H.M.J. contributed equally to this work. This research was supported by the Basic Science Research Program (CAFDC/K. J. Lee/No. 2013042126, NRF-2012R1A2A1A03010415), the Smart IT Convergence System of the Global Frontier Project (2012M3A6A6054187) funded by the Korean Government Ministry of Science, and ICT & Future Planning (MSIP) through the National

Research Foundation of Korea (NRF). Also, this work was supported by the Institute for Basic Science (IBS) in Korea, the Converging Research Center Program through the Korea Government MSIP (2012K001260).

[1] A. Kim, C. S. Ah, C. W. Park, J. H. Yang, T. Kim, C. G. Ahn, S. H. Park, G. Y. Sung, *Biosens. Bioelectron.* **2010**, *25*, 1767.
[2] F. Patolsky, G. F. Zheng, O. Hayden, M. Lakadamyali, X. W. Zhuang, C. M. Lieber, *Proc. Natl. Acad. Sci. USA* **2004**, *101*, 14017.
[3] L. A. Su, W. Z. Jia, C. J. Hou, Y. Lei, *Biosens. Bioelectron.* **2011**, *26*, 1788.
[4] I. Abdel-Hamid, D. Ivnitski, P. Atanasov, E. Wilkins, *Biosens. Bioelectron.* **1999**, *14*, 309.
[5] K. Ramanathan, B. Danielsson, *Biosens. Bioelectron.* **2001**, *16*, 417.
[6] R. S. Gaster, D. A. Hall, C. H. Nielsen, S. J. Osterfeld, H. Yu, K. E. Mach, R. J. Wilson, B. Murmann, J. C. Liao, S. S. Gambhir, S. X. Wang, *Nat. Med.* **2009**, *15*, 1327.
[7] T. D. Nguyen, N. Deshmukh, J. M. Nagarah, T. Kramer, P. K. Purohit, M. J. Berry, M. C. McAlpine, *Nat. Nanotechnol.* **2012**, *7*, 587.
[8] S. Y. Lee, K.-I. Park, C. Huh, M. Koo, H. G. Yoo, S. Kim, C. S. Ah, G. Y. Sung, K. J. Lee, *Nano Energy* **2012**, *1*, 145.
[9] C. L. Feng, X. H. Zhong, M. Steinhart, A. M. Caminade, J. P. Majoral, W. Knoll, *Adv. Mater.* **2007**, *19*, 1933.
[10] X. X. Duan, Y. Li, N. K. Rajan, D. A. Routenberg, Y. Modis, M. A. Reed, *Nat. Nanotechnol.* **2012**, *7*, 401.
[11] J. H. Ahn, S. J. Choi, J. W. Han, T. J. Park, S. Y. Lee, Y. K. Choi, *Nano Lett.* **2010**, *10*, 2934.
[12] Y. Cui, Q. Q. Wei, H. K. Park, C. M. Lieber, *Science* **2001**, *293*, 1289.
[13] W. Lu, P. Xie, C. M. Lieber, *IEEE Trans. Electron Dev.* **2008**, *55*, 2859.
[14] H. S. Im, X. J. Huang, B. Gu, Y. K. Choi, *Nat. Nanotechnol.* **2007**, *2*, 430.
[15] K. I. Chen, B. R. Li, Y. T. Chen, *Nano Today* **2011**, *6*, 131.
[16] A. R. Gao, N. Lu, P. F. Dai, T. Li, H. Pei, X. L. Gao, Y. B. Gong, Y. L. Wang, C. H. Fan, *Nano Lett.* **2011**, *11*, 3974.
[17] M. Im, J. H. Ahn, J. W. Han, T. J. Park, S. Y. Lee, Y. K. Choi, *IEEE Sens. J.* **2011**, *11*, 351.
[18] X. P. A. Gao, G. F. Zheng, C. M. Lieber, *Nano Lett.* **2010**, *10*, 547.
[19] M. L. Seol, J. H. Ahn, J. M. Choi, S. J. Choi, Y. K. Choi, *Nano Lett.* **2012**, *12*, 5603.
[20] S. Mao, G. H. Lu, K. H. Yu, Z. Bo, J. H. Chen, *Adv. Mater.* **2010**, *22*, 3521.
[21] A. Star, J. C. P. Gabriel, K. Bradley, G. Gruner, *Nano Lett.* **2003**, *3*, 459.
[22] F. Patolsky, G. F. Zheng, C. M. Lieber, *Nat. Protoc.* **2006**, *1*, 1711.
[23] S. Park, D. H. Lee, J. Xu, B. Kim, S. W. Hong, U. Jeong, T. Xu, T. P. Russell, *Science* **2009**, *323*, 1030.
[24] J. K. W. Yang, Y. S. Jung, J. B. Chang, R. A. Mickiewicz, A. Alexander-Katz, C. A. Ross, K. K. Berggren, *Nat. Nanotechnol.* **2010**, *5*, 256.
[25] K. Derbyshire, *Solid State Technol.* **2011**, *54*, 7.
[26] C. T. Black, R. Ruiz, G. Breyta, J. Y. Cheng, M. E. Colburn, K. W. Guarini, H. C. Kim, Y. Zhang, *IBM J. Res. Dev.* **2007**, *51*, 605.
[27] M. Park, C. Harrison, P. M. Chaikin, R. A. Register, D. H. Adamson, *Science* **1997**, *276*, 1401.
[28] T. Thurn-Albrecht, J. Schotter, C. A. Kastle, N. Emley, T. Shibauchi, L. Krusin-Elbaum, K. Guarini, C. T. Black, M. T. Tuominen, T. P. Russell, *Science* **2000**, *290*, 2126.
[29] S. O. Kim, H. H. Solak, M. P. Stoykovich, N. J. Ferrier, J. J. de Pablo, P. F. Nealey, *Nature* **2003**, *424*, 411.
[30] D. O. Shin, D. H. Lee, H. S. Moon, S. J. Jeong, J. Y. Kim, J. H. Mun, H. Cho, S. Park, S. O. Kim, *Adv. Funct. Mater.* **2011**, *21*, 250.
[31] R. Ruiz, H. M. Kang, F. A. Detcheverry, E. Dobisz, D. S. Kercher, T. R. Albrecht, J. J. de Pablo, P. F. Nealey, *Science* **2008**, *321*, 936.
[32] S. J. Jeong, G. D. Xia, B. H. Kim, D. O. Shin, S. H. Kwon, S. W. Kang, S. O. Kim, *Adv. Mater.* **2008**, *20*, 1898.
[33] B. H. Kim, D. H. Lee, J. Y. Kim, D. O. Shin, H. Y. Jeong, S. Hong, J. M. Yun, C. M. Koo, H. Lee, S. O. Kim, *Adv. Mater.* **2011**, *23*, 5618.
[34] X. Gu, Z. Liu, I. Gunkel, S. T. Chourou, S. W. Hong, D. L. Olynick, T. P. Russell, *Adv. Mater.* **2012**, *24*, 5688.
[35] B. Bhushan, D. R. Tokachichu, M. T. Keener, S. C. Lee, *Acta Biomater.* **2005**, *1*, 327.
[36] A. Hexemer, G. E. Stein, E. J. Kramer, S. Magonov, *Macromolecules* **2005**, *38*, 7083.
[37] S. J. Jeong, H. S. Moon, B. H. Kim, J. Y. Kim, J. Yu, S. Lee, M. G. Lee, H. Choi, S. O. Kim, *ACS Nano* **2010**, *4*, 5181.
[38] S. J. Jeong, J. E. Kim, H. S. Moon, B. H. Kim, S. M. Kim, J. B. Kim, S. O. Kim, *Nano Lett.* **2009**, *9*, 2300.
[39] K. G. A. Tavakkoli, K. W. Gotrik, A. F. Hannon, A. Alexander-Katz, C. A. Ross, K. K. Berggren, *Science* **2012**, *336*, 1294.
[40] E. Stern, J. F. Klemic, D. A. Routenberg, P. N. Wyrembak, D. B. Turner-Evans, A. D. Hamilton, D. A. LaVan, T. M. Fahmy, M. A. Reed, *Nature* **2007**, *445*, 519.
[41] H. J. Jang, W. J. Cho, *Appl. Phys. Lett.* **2012**, *100*, 073701.
[42] L. Gervais, N. de Rooij, E. Delamarche, *Adv. Mater.* **2011**, *23*, H151.
[43] E. P. Diamandis, T. K. Christopoulos, *Clin. Chem.* **1991**, *37*, 625.
[44] R. C. Duhamel, J. S. Whitehead, *Method. Enzymol.* **1990**, *184*, 201.
[45] M. L. Seol, S. J. Choi, C. H. Kim, D. I. Moon, Y. K. Choi, *ACS Nano* **2012**, *6*, 183.
[46] B. S. Doyle, S. Datta, M. Doczy, S. Hareland, B. Jin, J. Kavalieros, T. Linton, A. Murthy, R. Rios, R. Chau, *IEEE Electron Device Lett.* **2003**, *24*, 263.
[47] J.-P. Colinge, *FinFETs and Other Multi-Gate Transistors*, Springer, New York **2008**.

Received: April 19, 2013
Published online: July 24, 2013